Compact LTCC Dual-Mode Filter with Non-Orthogonal Feeding and Harmonics Suppression for 5G Applications

Changkun Li, Li Qian, Ziyang Zhang, Yunheng Wang, and Bo Zhou[*]

Abstract—A dual-mode band-pass filter (BPF) for the fifth generation (5G) N78 band applications is proposed based on a 2-layer low temperature cofired ceramic (LTCC) substrate. The proposed BPF is built with a square resonator and two pairs of open-stubs, which suppressed the 2nd-order and 3rd-order 27 and 21 dB, respectively. The proposed BPF not only achieved a size reduction of 50% compared with a single-mode implementation, but also possessed a non-orthogonal input/output (I/O) feeding style, which presents convenient interconnection and integration with neighboring devices. Moreover, the dual-mode BPF does not need a conventional disturbing element to excite two degenerate modes. Comparison and discussion are carried out as well.

1. INTRODUCTION

Nowadays, the fifth generation (5G) mobile communication has been on its business operation with high-speed and high-capacity data transmissions. The 5G communication requires to use sub 6 GHz frequency spectrum to transmit wideband signals. The most promising bands for 5G new radio (NR) in frequency range 1 (FR1) are N77 (3.3–4.2 GHz), N78 (3.3–3.8 GHz), and N79 (4.4–5 GHz) [1–3]. Therefore, there is an increasing requirement of 5G band-pass filters (BPFs), which can fulfill the needs of compact size, high integration, and good performances. Modern dual-mode BPFs achieve a size reduction of 50% compared with single-mode ones, but most of them use orthogonal feeding input/output (I/O) ports to excite two degenerate modes, which result in interconnecting difficulties with neighboring devices and higher in-band insertion loss with extra bend structure for transition [4–7]. In addition, modern communication transceiver is a nonlinear system, where the function of harmonics suppression is much preferred when designing modern BPFs. However, most of the recent dual-mode BPFs do not present the function of harmonics suppression [8, 9]. Extra low-pass filters may be required for harmonics suppression, which result in larger circuit size, higher cost, and complicated signal interference. Moreover, the conventional dual-mode BPF needs a disturbing element to excite two degenerate modes, and the disturbing element takes up circuit space and increases the optimization work of design.

In this paper, a dual-mode BPF is proposed for 5G N78 band applications. Owing to the LTCC technology, the I/O feeding lines with two pairs of open stubs and a square resonator are placed on different layers. The outer and inner open stubs are used to suppress the 2nd order and 3rd order harmonics, respectively. The merits of the proposed filter are 50% size reduction, 2nd-and 3rd-order harmonics suppression, non-orthogonal feeding, and no disturbing element needed.

2. FILTER DESIGN

2.1. Structure of the Proposed BPF

The structure of the proposed dual-mode BPF implemented on a 2-layer LTCC substrate is shown in Figure 1. The I/O feeding lines with two pairs of T-shaped open stubs are placed on the first layer, and the square ring resonator is placed on the second layer. The outer pair of lines with T-shaped open stubs is used to suppress the 2nd order harmonic, and the inner pair of lines with T-shaped open stubs is used to suppress the 3rd order harmonic. The structure of T-shaped open stubs has a low-pass characteristic, which can be used to suppress the high-order harmonics. The signal between the feeding lines and resonator is via broadband coupling effect, which also helps enhance the bandwidth of the proposed BPF. The bottom microstrip line is set to the ground layer.
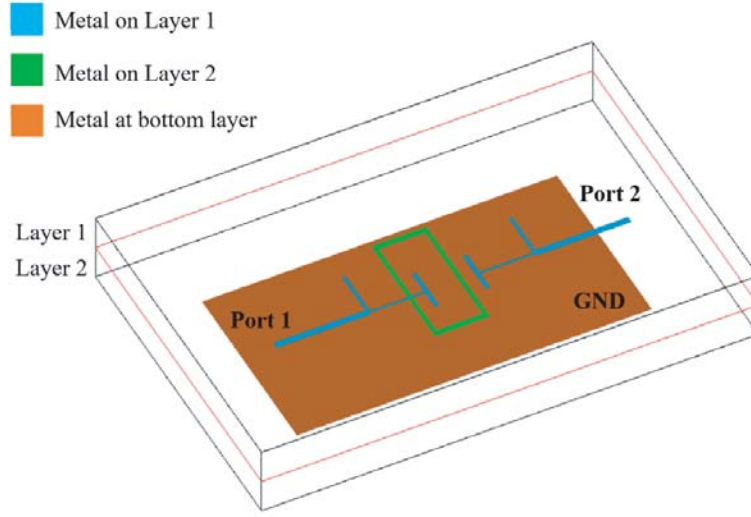
Figure 1. Structure of the proposed BPF.
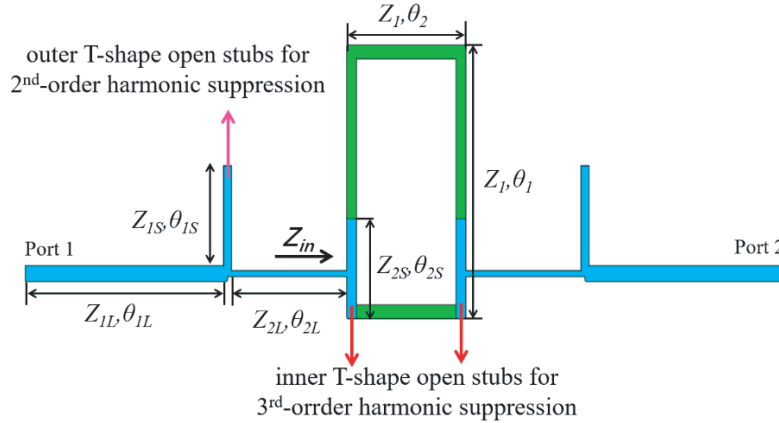
Figure 2. Schematic structure with impedance and electrical length definitions.

The impedance and electrical length of each section line are defined in Figure 2. As the I/O feeding line is constructed with 2-stage cascaded T-shaped open stubs, the total impedance of the I/O feeding line can be obtained by ABCD parameters [5], which are given by

$$Z_{nL} = \frac{Z_1}{\tan \theta_{nL}} \tag{1}$$

$$Z_{nS} = \frac{Z_1 \tan \theta_{nS}}{1 - \tan^2 \theta_{nL}} \tag{2}$$

where Z_1 is the impedance of the square ring resonator. Z_{nL} and θ_{nL} are the impedance and electrical length of each horizontal I/O feeding section, respectively. Also, Z_{nS} and θ_{nS} are the impedance and electrical length of each vertical open stub, respectively.

2.2. Circuit Analysis

Since the structure of the proposed BPF is symmetrical, even- and odd-modes can be used for the analysis. The vertical and horizontal strip-lines of the square ring resonator on Layer 2 have electrical lengths of θ_1 and θ_2, respectively. The characteristic impedances of vertical and horizontal strip-lines are both Z_1. An electric wall is applied along the symmetric plane and divides the structure into one-half. Figures 3(a) and (b) present the equivalent even- and odd-mode circuits, respectively. The input characteristic impedance of the resonator is Z_{in}, and the even- and odd-mode characteristic impedances of the vertical broadside-coupled line are Z_{1o} and Z_{1e}, respectively. By calculating the input impedances Z_{odd} and Z_{even} of the transmission line, the transmission and reflection coefficients of 2-port ring resonator can be given by [10]

$$S_{11} = \frac{Z_{even}Z_{odd} - Z_{in}^2}{(Z_{odd} + Z_{in})(Z_{even} + Z_{in})} \tag{3}$$

$$S_{21} = \frac{Z_{even}Z_0 - Z_{odd}Z_{in}}{(Z_{odd} + Z_{in})(Z_{even} + Z_{in})} \tag{4}$$

The following equation having an electrical length θ_t can be obtained when the numerator of Equation (4) is zero and then can derive impedances Z_{1o}, Z_{1e} and Z_2 by

$$(\alpha + 1) \cos^4 \theta_t - 2\alpha \cos^2 \theta_t + \alpha - 1 = 0 \tag{5}$$

$$\alpha = \frac{Z_{1o} + Z_{1e}}{2Z_2} \tag{6}$$

Equation (5) shows that the electrical θ_t is determined by the impedance ratio α defined in Equation (6). Then, the resonator's response can be predicted.
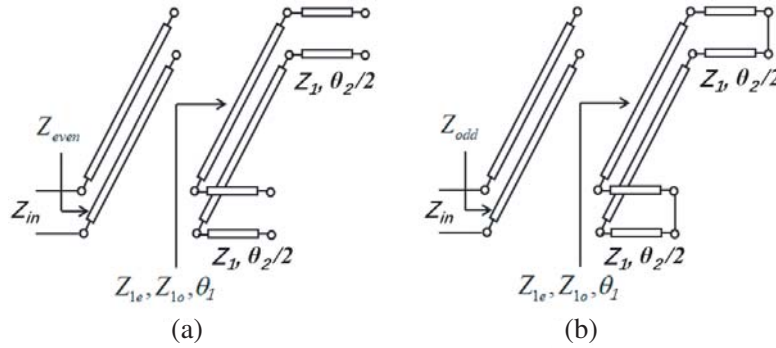
Figure 3. (a) Even-mode circuit and (b) odd-mode circuit.

2.3. Key Parameters' Design

The dimension parameters are defined in Figure 4. To guarantee a satisfied performance, various dimension parameters (w_1, w_4, w_5, and l_3) are simulated and verified with EM-simulations. To obtain a wideband response and impedance matching to cover N78 band, the width of ring resonator is a key parameter for BPF's design. Figure 5 displays the BPF's return loss responses with varied width w_4 and w_5 of ring resonator. As depicted in Figure 5, the proper width of ring resonator does help the BPF
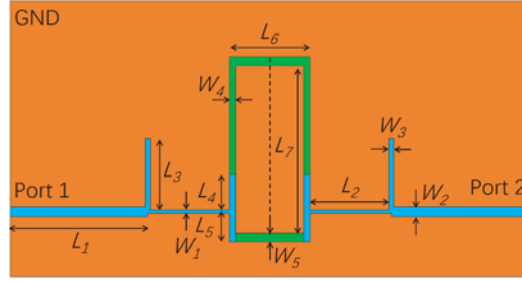
Figure 4. Plane geometry with parameters' definitions.
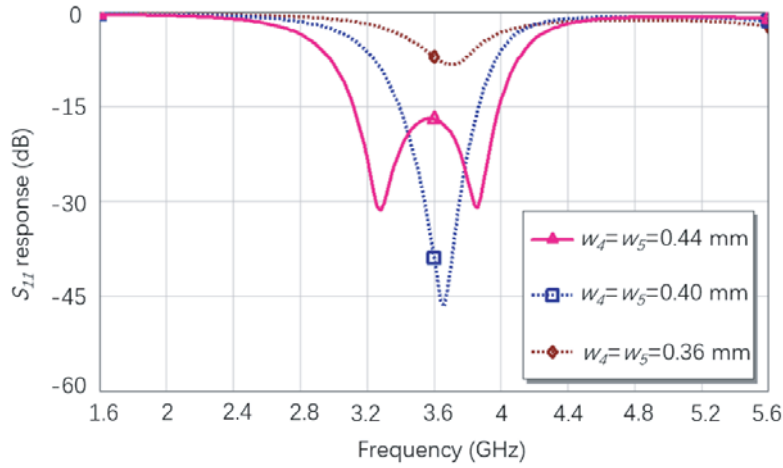
Figure 5. Return loss responses of the BPF with varied parameters of w_4 and w_5.
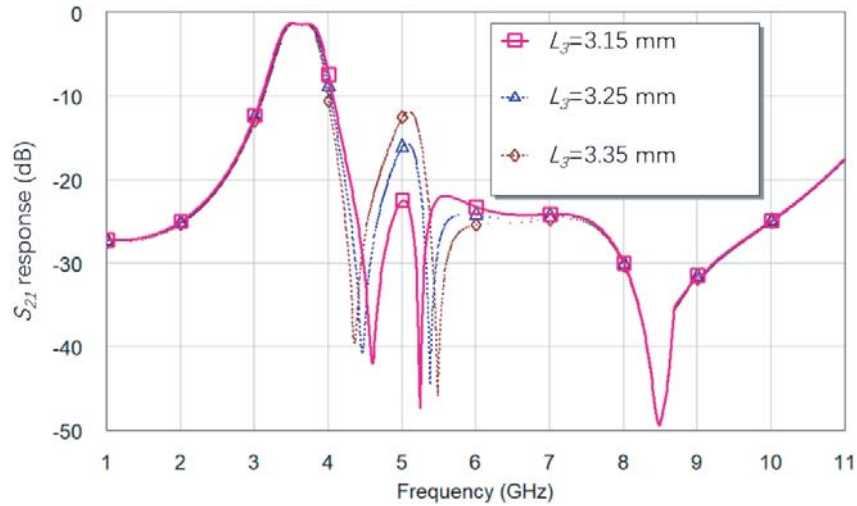
Figure 6. Insertion loss responses of the BPF with varied parameters of L_3.

broaden its bandwidth. Figure 6 shows the BPF's insertion loss responses with varied length L_3. As can be seen in Figure 6, when L_3 increases, the signal suppressions at 5 GHz become worse. Similarly, as shown in Figure 7, when a larger w_1 is given, a higher in-band ripple is observed, and signal suppression is also getting worse. Thus, the parameters of ring resonator and T-shaped structure play significant roles in boosting the in-band ripple and out-of-band suppression performance of the BPF.
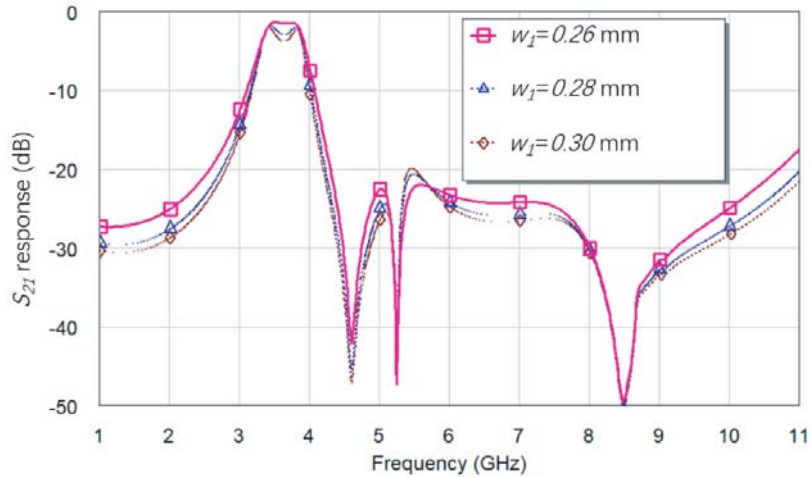
Figure 7. Insertion loss responses of the BPF with varied parameters of w_1.

Following the above discussion, the proposed BPF with two pairs of T-shaped structures exhibits a great sideband performance, whereas its stopband region extends over $3f_0$ with 21 dB signal suppression.

3. SIMULATED AND MEASURED RESULTS

An AXIEM solver [11] based on the full-wave electromagnetic (EM) simulation is used for EM-optimization. The dimension parameters are defined in Figure 4, and the optimal dimensions are listed in Table 1. A photograph of the proposed BPF is shown in Figure 8. Ground-signal-ground (GSG) pads are reserved at the I/O ports for probe measurements. Measurements are carried out by Agilent N5230C network analyzer and Cascade Microtech Summit 9000 probe stations with 400 μm-GSG probes, shown in Figure 9. The measured results agree well with the simulated ones, as shown in Figure 10. From the

Table 1. Dimensions of the proposed filters (unit: mm).

Parameter	L_1	L_2	L_3	L_4	L_5	L_6
Value	4.68	2.05	3.15	194	1.55	1.88
Parameter	L_7	W_1	W_2	W_3	W_4	W_5
Value	5.66	0.26	0.72	0.35	0.44	0.44
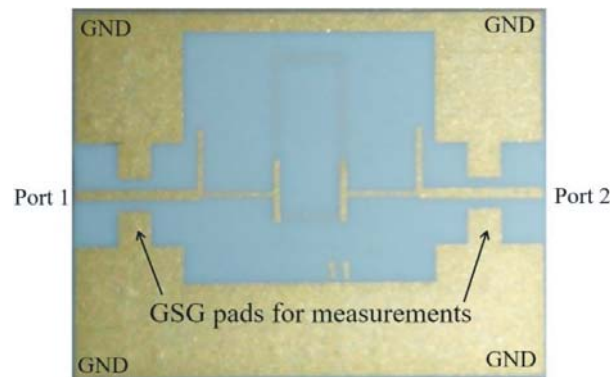
Figure 8. Photograph of the proposed BPF.
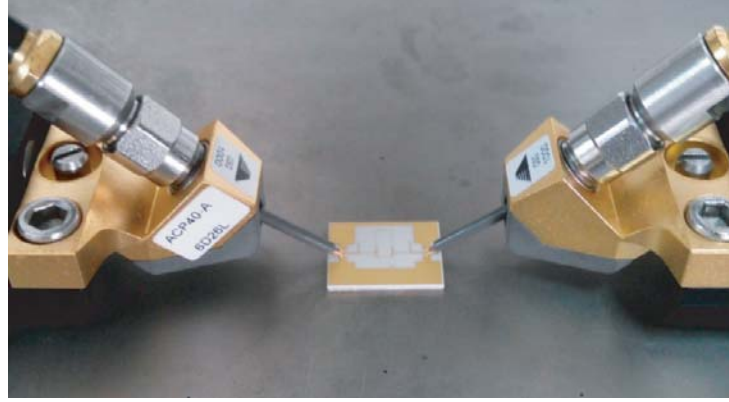
Figure 9. Photograph of the measurements.
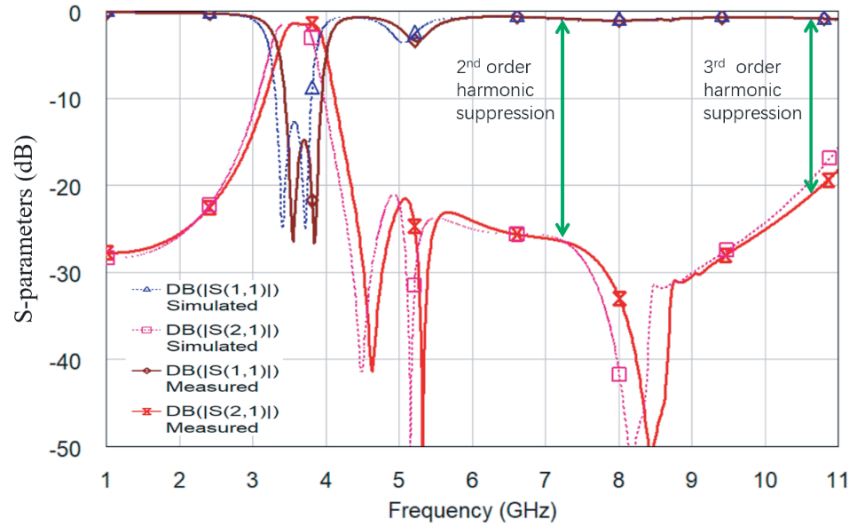
Figure 10. Simulated S-parameters of the proposed BPF.

measurement, the BPF has a center frequency of 3.59 GHz (simulated center frequency is 3.55 GHz), as well as a fractional bandwidth (FBW) of 14% with return loss better than 16 dB. The tiny frequency shift of 0.04 GHz is caused by the ceramic shrinking after cofiring. The measured insertion loss (IL) is better than 1.1 dB within the passband. Noticeably, the prototype BPF exhibits a wide stopband region from 4.2 GHz to 10.8 GHz (that is $3f_0$) with a high rejection level of 21 dB. The suppression of the 2nd order and 3rd order harmonics is 27 and 21 dB, respectively. The size of the proposed BPF is only 5.98 mm × 5.66 mm (the length L_1 part in Figure 4 is ignored as it is 50 Ω I/O line for measurement), which achieves a size reduction of 50% compared with a single-mode implementation.

4. COMPARISON AND DISCUSSION

Comparison results between the proposed BPF and existing designs are summarized in Table 2. The overall performances of the proposed BPF exceed the performances of existing BPFs in terms of insertion loss, harmonic suppression, and I/O feeding style [4–7]. The proposed BPF has the lowest in-band insertion loss, highest harmonics suppression levels, and non-orthogonal I/O feeding style, which is easily interconnecting and integrating with neighboring devices. The broadside coupling between the inner T-shaped stubs and the square ring resonator also helps enhance the bandwidth. The proposed

Table 2. Performance comparison.

Refs.	Center frequency	In-band insertion loss	2nd order harmonic suppression (dB)	3rd order harmonic suppression (dB)	I/O feeding style	Geometry complexity	Fabrication process
[4]	2.59	4.5	22	10	orthogonal	high	PCB
[5]	2	2.6	15	12	orthogonal	middle	PCB
[6]	1.575	2	25	15	orthogonal	high	PCB
[7]	1.2	1.5	15	13	orthogonal	high	PCB
This work	3.55	1.1	27	21	non-orthogonal	low	LTCC

dual-mode BPF is only $5.98\,\text{mm} \times 5.66\,\text{mm}$, which achieves a size reduction of 50% compared with a single-mode implementation. Moreover, the proposed BPF owns an uncomplicated geometry with neither vias nor intricate stirps, and uses only two layers in an LTCC substrate. Accuracy and stability are ensured, and a good potential to be highly integrated and massively installed in a compact Ericsson 5G base station is achieved. The proposed BPF has already been equipped in Ericsson 5G base stations.

5. CONCLUSION

An LTCC based dual-mode BPF for 5G N78 band application is proposed and verified. The proposed BPF has the advantages of size reduction, harmonics suppression, and non-orthogonal I/O feeding style. Comparison shows that the proposed BPF has better performance than existing BPFs. The measured results agree with the simulations well. The proposed BPF has a simple structure, which will be excellent for 5G mass production with a higher yield, and it has already been equipped in Ericsson 5G base stations.

ACKNOWLEDGMENT

REFERENCES

1. Okuyama, Y. S. S. and N. I. T. Takada, "5G radio performance and radio resource management specifications," 2019.

2. Shin, K. R. and K. Eilert, "Compact low cost 5G NR n78 band pass filter with silicon IPD technology," *Proc. 2018 IEEE 19th Wireless and Microwave Technology Conference (WAMICON)*, 1–3, 2018.

3. Okuyama, Y. S. S. and N. I. T. Takada, "5G radio performance and radio resource management specifications," 2019.

4. Hu, W., T. Yoshimasu, and H. Liu, "A novel dual-mode square loop passband filter with second spurious passband suppression," *Proc. IEEE International Conference on Communications, Circuits and Systems*, Vol. 4, 2273–2276, 2006.

5. Jeon, B. K., H. Nam, K. C. Yoon, B. W. Jeon, Y. W. Kim, and J. C. Lee, "Design of a patch dual-mode bandpass filter with second harmonic suppression using open stubs," *Proc. IEEE Asia-Pacific Microwave Conference*, 1106–1109, 2010.

6. Kuan, H. and H.-Y. Pan, "Design of a dual-mode bandpass filter with wide stopband performance for GPS application," *Microwave Opt. Technol. Lett.*, Vol. 50, No. 2, 445–447, 2008.

7. Karpuz, C. and A. K. Gorur, "A novel compact configuration for dual-mode microstrip resonators and dual-band bandpass filter applications," *Microwave Opt. Technol. Lett.*, Vol. 55, No. 4, 775–779, 2013.

8. Zhu, J.-M., et al., "Compact high-selectivity tunable dual-mode filter with constant bandwidth by adopting frequency-dependent S-L coupling," *Microwave Opt. Technol. Lett.*, Vol. 62, No. 1, 108–111, 2020.

9. Cheng, Y., C. Mei, and L. Zhu, "Design of dual-mode band-pass filter with novel perturbation elements," *Progress In Electromagnetics Research C*, Vol. 96, 59–71, 2019.

10. Zhou, B., et al., "Wide upper stopband and nonorthogonal I/O feed dual-mode LTCC filter," *Proc. IEEE International Symposium on Radio-Frequency Integration Technology (RFIT)*, 1–3, 2016.

11. AXIEM, Applied Wave Research Corporation, El Segundo, CA.